Available online at www.sciencedirect.com
SCIENCE DIRECT®
Journal of Sound and Vibration 290 (2006) 48–64
JOURNAL OF SOUND AND VIBRATION
www.elsevier.com/locate/jsvi

Anti-symmetric mode vibration of a curved beam subject to autoparametric excitation

Y.Y. Lee[a,*], W.Y. Poon[b], C.F. Ng[b]

[a]*Department of Building and Construction, City University of Hong Kong, Kowloon Tong, Kowloon, Hong Kong*
[b]*Department of Civil and Structural Engineering, Hong Kong Polytechnic University, Hung Hom, Kowloon, Hong Kong*

Received 5 July 2004; received in revised form 24 February 2005; accepted 14 March 2005
Available online 19 July 2005

Abstract

This paper details study of the antisymmetric response to the symmetric sinusoidal excitation of a clamped–clamped buckled beam. The autoparametric responses of the antisymmetric modes are obtained from a two-mode equation with nonlinear coupling, which is solved using the Runge–Kutta numerical integration method. The effects of the antisymmetric mode vibration on the dynamic snap-through motion are studied. The theoretical results conclude that (i) the autoparametric responses occur for large static buckled shapes when the resonance frequency of the symmetric mode is about twice that of antisymmetric mode, (ii) autoparametric responses are dominant at a frequency that is half that of the excitation, (iii) the autoparametric responses of antisymmetric modes are as high as the symmetric mode although the excitation force is symmetric, and the autoparametric responses decrease the excitation force that is required to initiate the dynamic snap-through motion. The experimental results for a buckled beam were obtained by base excitation with a 6000 N shaker. The measurement of the antisymmetric modes was separated from the measurement of the symmetric mode by the special configuration of the strain gauge sensor systems. A comparison of the simulation results and the measured data shows a reasonable agreement, and demonstrates the effectiveness of the modeling approach.

*Corresponding author. Fax: +852 27788 7612.
E-mail address: bcraylee@cityu.edu.hk (Y.Y. Lee).

0022-460X/$ - see front matter © 2005 Elsevier Ltd. All rights reserved.
doi:10.1016/j.jsv.2005.03.009

1. Introduction

It is well known that the static stability of an initial symmetric buckled mode is significantly affected by the onset of antisymmetric displacement, but the dynamic effects of antisymmetric modes on the snap-through motion are less well understood. Previous theoretical studies [1–3] have shown that antisymmetric modes can be excited by symmetric excitations, which are known as autoparametric responses. However, limited experimental results have been obtained to verify this phenomenon.

The nonlinear interaction of a multi-degree of freedom system with internal resonance was studied by Chang et al. [4]. Afaneh and Ibrahim [5] found that the first mode transfers energy to the second mode when the first mode is externally excited around a small frequency range in the neighborhood of the 1:1 internal resonance. The parametric excitation of a beam-pendulum that has two degrees of freedom has been studied, and shows an energy transfer between the two modes. The energy transfer phenomenon is called autoparametric resonance or autoparametric instability. Detailed discussions on this subject can be found in the work of Nayfeh and Mook [6]. More recently, the parametric analysis of a beam that is subjected to a time-dependent compressive axial load was carried out by Liao and Huang [7] and Tan et al. [8]. However, these studies were limited to a spinning pre-twisted beam, although they demonstrated that a chaotic motion appears in the neighborhood of the stability limit of the parametric excited resonance and triggers the first mode snap-through motion.

The equation of motion of a buckled beam is governed by the Duffing equation with a negative linear stiffness and a softening-type cubic equation nonlinearity. A Rayleigh–Ritz analysis using a single-mode model to represent the transverse displacement of a plate due to in-plane stress was developed by Ng [9–12]. The response showed the characteristic of nonlinear phenomena including bifurcation, fundamental, subharmonic, and superharmonic resonances, and chaotic behavior. Afaneh and Ibrahim [13] and Kreider and Nayfeh [14] experimentally investigated the response of a fixed–fixed buckled beam under sinusoidal excitation, and Afaneh and Ibrahim [13] analyzed the first three modes of a curved beam under sinusoidal loads. The equations of motion were derived using the Galerkin's method and the stability analysis was performed using the Hopf bifurcation procedures.

In this study, the equations of motion for a clamped–clamped curved beam subjected to transverse sinusoidal loads are derived using the assumed mode and Galerkin method. The fundamental mode of vibration of the beam is symmetric, whereas the second mode is antisymmetric. In addition to the effect of the symmetric mode, the effect of parametric excitation near the symmetric mode resonance frequency is studied. Due to the presence of the antisymmetric mode, under certain conditions, the excitation force that is required for the onset of the snap-through is less than that required in the single-mode approach.

The experimental results for a buckled beam were obtained by base excitation with a 6000 N shaker. The measurement of the antisymmetric modes was separated from the measurement of the symmetric mode by the special configuration of the strain gauge sensor systems. The test results are in good agreement with the predicted autoparametric responses.

Compared to the classical single-mode parametrical excitation, the primary region of autoparametric responses occurs under lower forces and a wider range of excitation frequencies.

Thus, autoparametric systems display the interesting physical behavior, but also have an impact on practical structures that may react dangerously to small periodic excitations.

2. Two-mode equations for the nonlinear coupling of a beam

The system under investigation is shown schematically in Fig. 1. Consider a clamped–clamped beam of width a and length L in the x-direction with thickness d. The plate is subject to horizontal displacement U in the x-direction. The end moves only during the initial compression process and is fixed for dynamic loading. By using Hamilton's principle, the governing differential equation of a clamped–clamped beam that is subjected to a uniaxial static load P and a transverse harmonic support motion $y = Y_0 \sin \omega_f t$ is

$$m\left(\frac{\partial^2(w(x,t)+w_o(x))}{\partial t^2}+\frac{\partial^2 y(t)}{\partial t^2}\right)+c\frac{\partial(w(x,t)+w_o(x))}{\partial t}+EI\frac{\partial^4(w(x,t)+w_o(x))}{\partial x^4}$$
$$+P\frac{\partial^2(w(x,t)+w_o(x))}{\partial x^2}-\frac{EA}{2L}\frac{\partial^2(w(x,t)+w_o(x))}{\partial x^2}\int_0^L\left(\frac{\partial(w(x,t)+w_o(x))}{\partial x}\right)^2 \mathrm{d}x=0, \quad (1)$$

$$P=\frac{4\pi^2 EI}{L^2}+\frac{EA}{2L}\int_0^L\left(\frac{\partial w_o(x)}{\partial x}\right)^2 \mathrm{d}x, \quad (2)$$

where m is the mass per unit length, w is the transverse displacement of the beam, E is the Young's modulus, A is the cross-sectional area of the beam and I is the moment of inertia of bending, L is the length of the buckled beam, P is the initial axial load which is greater than the Euler buckling load, and c is the damping coefficient.

Assuming the appropriate shape functions for the transverse displacement of the beam and using Galerkin's procedure of formulation, the nonlinear coupling equations of dynamic motion for the first two-mode vibration in the transverse direction are obtained. The detailed steps for deriving the following formulas are found in Poon et al. [15]:

$$\frac{\ddot{q}_1}{\Omega^2}+\frac{2\xi}{\Omega}\dot{q}_1-R_1 q_1+q_1^3+4.526 q_1 q_2^2=p, \quad (3)$$

$$\frac{\ddot{q}_2}{\Omega^2}+\frac{2\xi}{\Omega}\dot{q}_2+(7.5-2.808R_1)q_2+12.712q_2^3+2.808q_1^2 q_2=0, \quad (4)$$

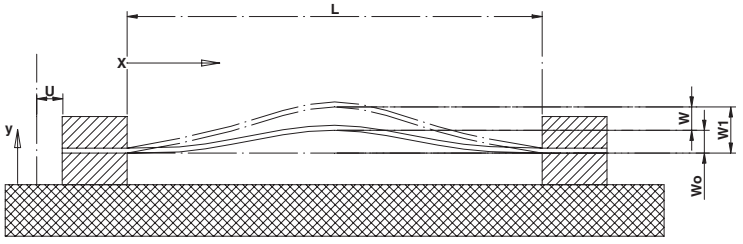

Fig. 1. Illustration of clamped–clamped beam model.

$$p = \frac{1.154\omega_f^2}{R_1\Omega^2 t} Y_0 \sin \omega_f t, \tag{5}$$

where $\xi = c/2m\Omega$, Ω is the linear circular frequency of the flat beam, $R_1 = \lambda - 1$ (buckling parameter), $\lambda = U/U_c$, U is the in-plane edge shortening displacement, U_c is the value of U at which buckling starts, q is the nondimensional displacement parameter (w_1/w_N at $x = L/2$), w_1 is the modal displacement, w_N is the value of w_1 at $R = 1$, and ω_f is the excitation frequency.

3. Experimental results

3.1. Test setup

A test beam of breadth $a = 52.0$ mm, thickness $t = 1.5$ mm, and effective length $L = 355.0$ mm (the total length including the clamped portions is 410 mm) was fabricated from an aluminum alloy sheet. The Young's modulus was $E = 71.6 \times 10^9\,\mathrm{N/m^2}$ and the mass density is $\rho = 2700\,\mathrm{kg/m^3}$. Based on this data, the first mode and second mode linear natural frequency can be obtained by

$$\omega_i = C_i \sqrt{\frac{EI}{mL^4}},$$

where ω_i is the linear natural frequency of the flat beam at i mode. $C_1 = 3.56$, $C_2 = 9.82$.

The corresponding natural frequency for the first mode is 64.8 Hz and for the second mode is 178.7 Hz. However, the inevitable slipping effect at the clamps causes a deviation in natural frequency response. Later sections of this paper will mention the actual natural frequencies that are obtained by the frequency response test.

As shown in Figs. 2 and 3, the clamped portion of the beam is stiffened with a pair of 25 mm thick aluminum bars and two 9 mm diameter stainless-steel bolts, which are firmly fixed to the

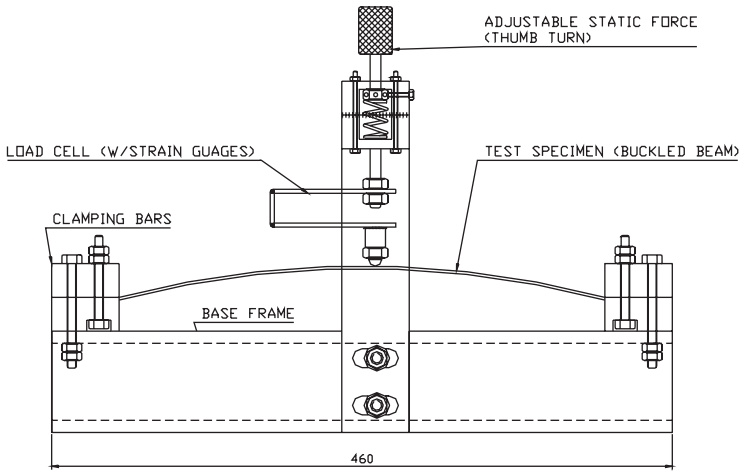

Fig. 2. Test rig for clamping the beam with in-plane compression.

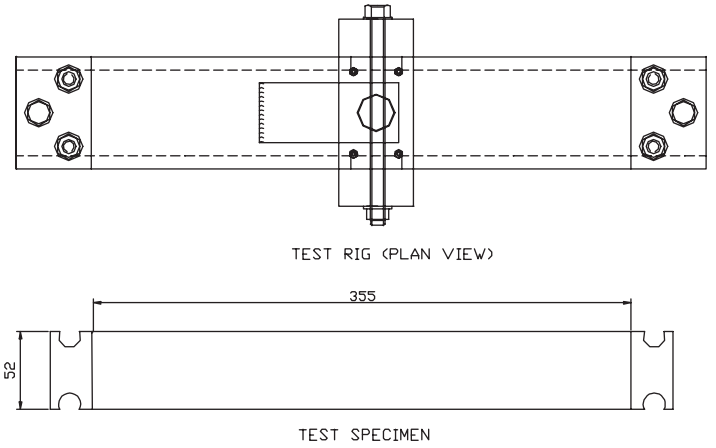

Fig. 3. Top view of the test rig and the specimen for static testing.

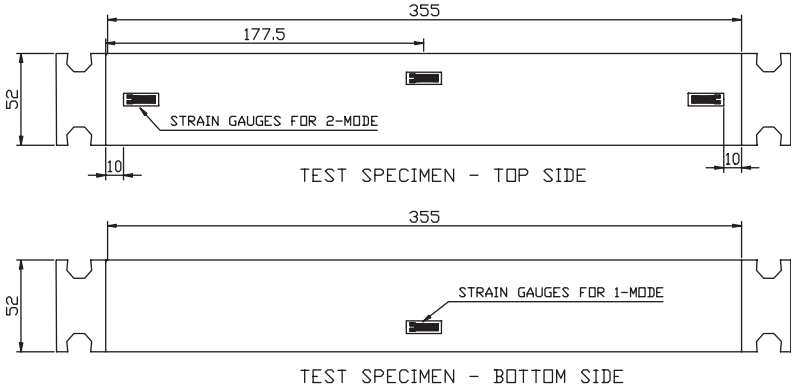

Fig. 4. Test beam mounted with strain gauges to measure the first and second modes.

aluminum base frame by one 12-mm-diameter bolt. The base frame for the static testing is an aluminum hollow box section tube that is 75 mm wide × 75 mm high × 4.5 mm thick with a total length of 460 mm.

To reduce the effect in the dynamic test of the resonance frequency that is due to the base frame, the frame was replaced with a thick solid bar that was 75 mm wide × 30 mm high × 480 mm long. The base frame was bolted to the exciter table of the vibration shaker. By shaking the base frame sinusoidally at frequency ω and peak acceleration a_b (g), a uniformly distributed pulsating load $P \sin \omega t$ was applied to the beam with a loading amplitude of $P = \rho\, a\, t\, a_b$ (N/m).

Tests were conducted by periodically exciting the base frame of the beam and measuring the relative displacement of the beam to the frame using strain gauges as sensing elements. The

mounting of the test beam on the shaker and the arrangement of the transducers are shown in Figs. 2 and 4.

A measure of the response was obtained from a pair of strain gauges that were located at $x/L = 0.5$, where x is the distance along the clamped end. Two back-to-back strain gauges (on two sides of the beam) were glued to the middle of the beam, and another pair of strain gauges (on two sides of the beam) was mounted at the ends ($x/L = 0.029$ and $x/L = 0.971$). The first pair of strain gauges corresponded to the first mode, in which the strains that were due to the second mode were cancelled out. For the same reason, the second pair of strain gauges measured the second mode strains only. The gauge factor of the strain gauges at 24 °C was 2.090, and the resistance was 350 Ω. Each pair of gauges was attached to a half-bridge connection of a bridge amplifier and meter (Measurement Group Instruments Division model: BAM-1B). The DC output data that were acquired from the two strain meters was then monitored by a dual-channel signal analyzer. The displacement responses were measured in terms of bending strains, and a constant scaling factor was applied to the strains to convert them into amplitudes. A piezoelectric accelerometer was used to monitor the acceleration of the shaker table. The base frame was bolted to the shaker table of a 6000 N "LING" electromagnetic shaker. A schematic diagram of the whole setup is shown in Fig. 5.

With this arrangement, the sweeping sine-wave excitation of the frame could be carried out for a wide frequency range, with the peak acceleration being kept constant at the predetermined level. The maximum dynamic force of the shaker was about 6 kN (611 kgf). The workload (base frame plus test beam) was 4.36 kg, and the maximum G attachable for the workload was 140 G. The

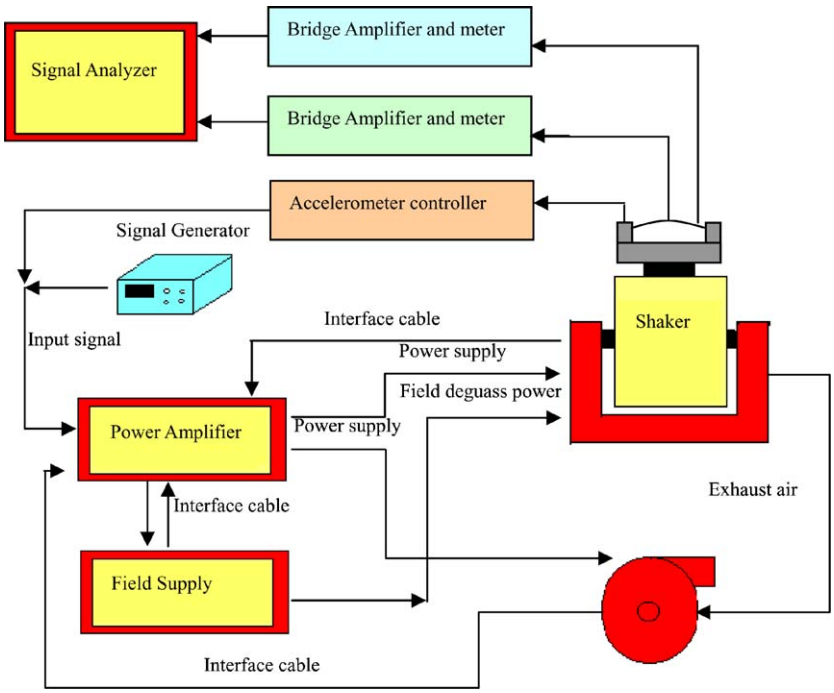

Fig. 5. Schematic diagram of the dynamic test set-up.

instrumentation obtained a signal that was proportional to the relative displacements of the beam both for the symmetric mode and the antisymmetric mode. A dual-channel analyzer was used to monitor and record the waveforms of the beam responses.

3.2. Static test

Before conducting a dynamic test to identify the effects of the antisymmetric mode, a static compression test was implemented to obtain the data for the basic parameters. As shown in Fig. 2, a loading rig that facilitated the transverse displacement of the beam was designed for the static test. Clamped–clamped boundary conditions had to be satisfied by two clamping bars that were mounted on a hollow box section base frame. Two double-nut lock screws were used for the clamping and sliding movement in a slot on the base frame.

In the static test, a frequency response measurement was also conducted to understand the first and second natural frequencies under various curvatures. A Brüel & Kjaer impedance head 8001 was used as a forcing hammer and a Brüel & Kjaer accelerometer 4374 was fixed on the beam to pick up the responses. A dual-channel Hewlett Packard 3569A real-time frequency analyzer was used as the analyzing tool.

The experimental values of R_1 for different beam center displacements were found by plotting the deflection against the static load and using the curve-fitting technique to find the corresponding cubic equations. The results are tabulated in Table 1 and Fig. 6. The experimental values of R_1 were compared with the theoretical value of R_1, and were found to be in good agreement with each other when R_1 is smaller than 4.

To find the spatial distribution of the transverse static displacement in a beam that is due to a compressive vertical load, the deflections of 10 evenly distributed points were marked and measured for different static loads. The spatial distribution of the buckled beam is shown in Fig. 7. The pattern gives an indication of the static modes of displacement as they changed from the first mode to the second mode by observing the points of maximum displacement (crests or troughs). The second mode becomes predominant when the buckling parameter is large (greater than 4.0), which satisfies the conditions for the occurrence of the second mode as predicted by the equations.

Table 1
List of experimental and theoretical R_1 with Center Displacement

Displacement W_1 (mm) (center of the beam)	R_1 (by curved fitting)	R_1 (by calculation)
9.4	45.42	29.45
8.2	37.73	22.41
5.2	11.9	9.01
4.1	6.12	5.70
3.3	3.47	3.63
2.8	2.12	2.61
2.1	1.06	1.47
1.5	−1.27	0.75

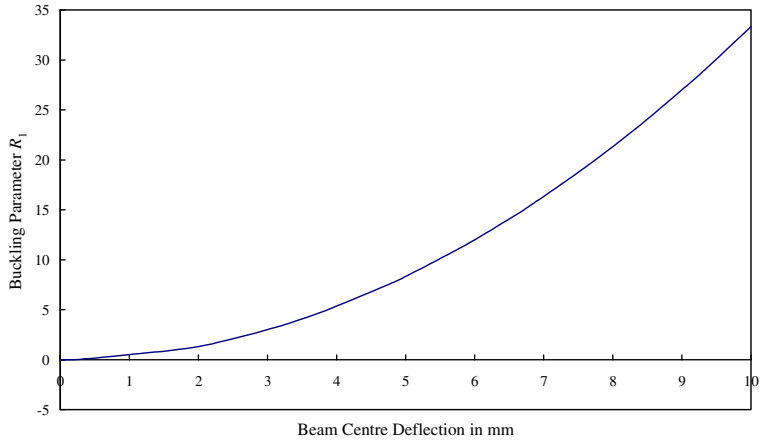

Fig. 6. Relationship between the initial static deflection and buckling parameter.

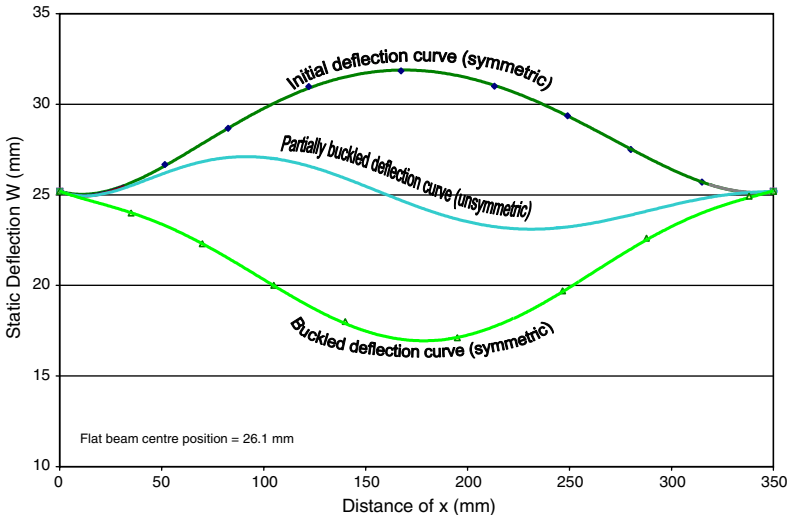

Fig. 7. Spatial deflection curves for the beam under $R_1 = 17.28$.

The discrepancy in R_1 between the experiment and the calculations was large when the initial static deflection was greater than four times the thickness of the beam, which is verified by Table 1. The discrepancy may have arisen because of the occurrence of a second mode (modal interaction) for large R_1, because of the geometric imperfection of the beam, or because the clamping bars at either end may not have securely held the beam in a horizontal position under a large in-plane compression force (imperfect boundary clamping or in-plane slippage: there may have some tilting at the clamping bars that changed the boundary conditions of the beam).

For a highly accurate solution to the buckling parameter, the displacement to thickness ratio has to be limited to 4.

3.3. Frequency response test

In the impact test, the natural frequencies for the first two modes were identified with different curvatures, and were close to the calculated frequencies for the flat beam. The third mode and torsional (twisting) mode also appear in the frequency response diagrams. Fig. 8 shows the linear natural frequency for the first two modes against the beam center deflection. The experimental and theoretical frequency ratios ω/Ω for the first and second modes are indicated in Fig. 9. The experimental impact tests showed a shifting in the natural frequency of the flat beam due to

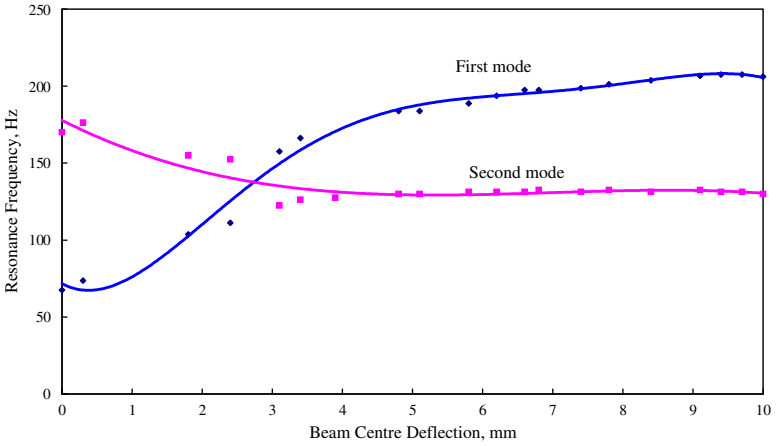

Fig. 8. Experimental relationship between the linear resonance frequency and beam center deflection.

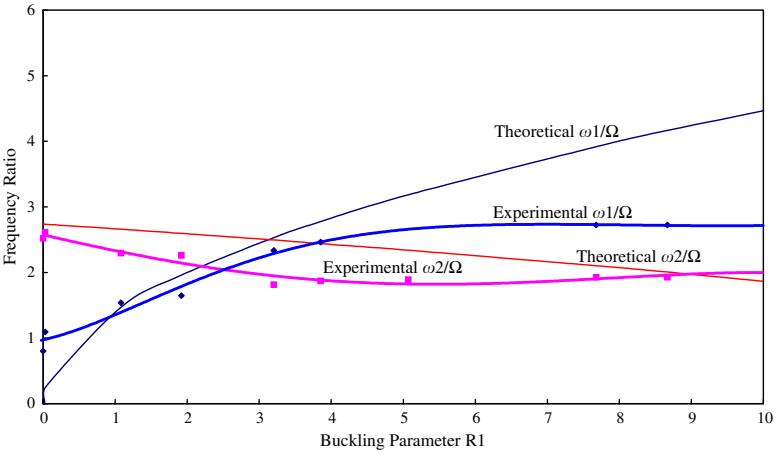

Fig. 9. Experimental and theoretical frequency ratios of the first and second modes.

inevitable slipping at both ends. Hence, the beam center deflection value was measured before and after each measurement to obtain the average value. The presence of imperfection also caused a deviation.

3.4. Dynamic test by frequency sweep

Taking the dimensions and material properties of the test beam into consideration, the experiments were carried out by taking the peak acceleration of the base frame as $a_b = 60g$ and varying the excitation frequency from 30 to 300 Hz.

The dynamic responses in terms of the bending strain were measured at the midpoint and endpoint of the beam under flat and varying beam curvatures (2.8 and 3.5 times the thickness of the beam). The bridge amplifiers were balanced, and the gain was properly adjusted to the dynamic range. To alter the initial axial displacement (beam curvature) with a clamp, the central portion of the beam was buckled. At the prescribed curvature, detailed tests were conducted to clarify the frequency spectrum and waveform of the responses with the set-up that is shown in Fig. 5. The DC data on the time histories, mean, and root mean square frequency response were measured and recorded with excitation levels of $1g$, $4g$, $16g$, $32g$ and $60g$. The frequencies that started with a snap-through were recorded, and the same procedure was repeated at various curvatures.

4. Comparison of the experimental and theoretical results

To examine the instability region, the numerical results for the two cases were compared to those that were directly measured from the testing rig for the same conditions. Figs. 10–13 show the response signals at excitation levels of $1g$ to $32g$ against frequencies that range from 30 Hz to

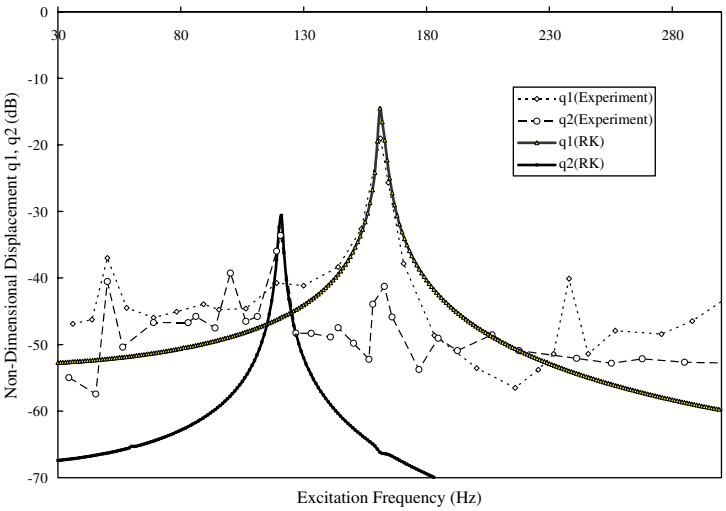

Fig. 10. Modal responses of 4.1 mm ($R_1 = 5.7$) at $1g$.

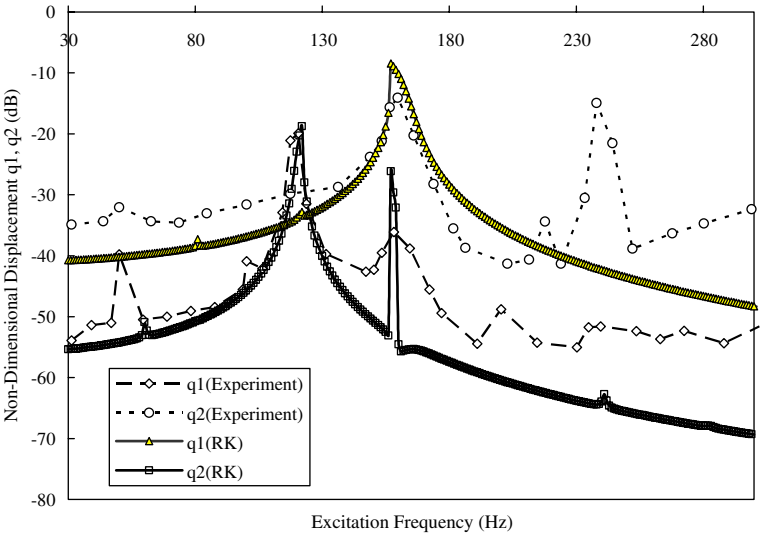

Fig. 11. Modal responses of 4.1 mm ($R_1 = 5.7$) at $4g$.

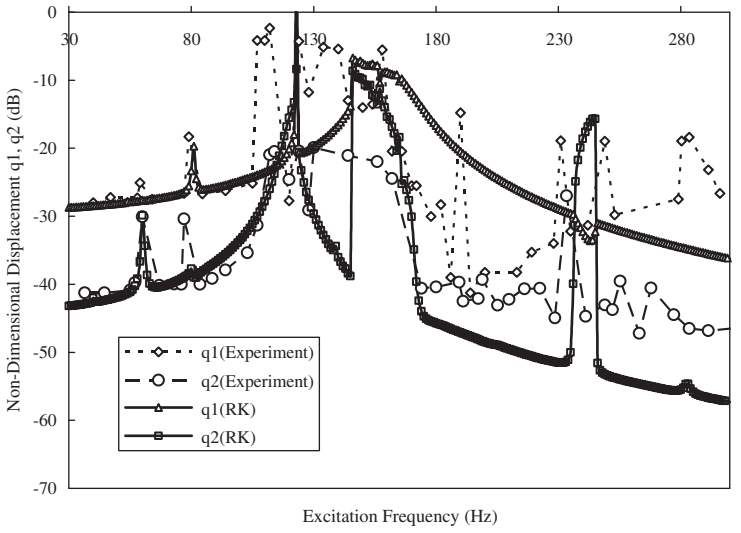

Fig. 12. Modal responses of 4.1 mm ($R_1 = 5.7$) at $16g$.

300 Hz. The nonlinear natural frequency ratio between the first two modes (symmetric and antisymmetric modes) for a 4.1-mm ($R_1 = 5.7$) deflection is 1.35. The second mode is coupled to the primary mode in a nonlinear manner, and the antisymmetric mode is parametrically excited at 163 Hz, which is the resonant frequency of the symmetric mode. Figs. 10–13 show that the nonlinear coupling starts both at 121 Hz and 163 Hz, and that the system becomes unstable near these intervals of the frequency of the excitation. The autoparametric instability is not

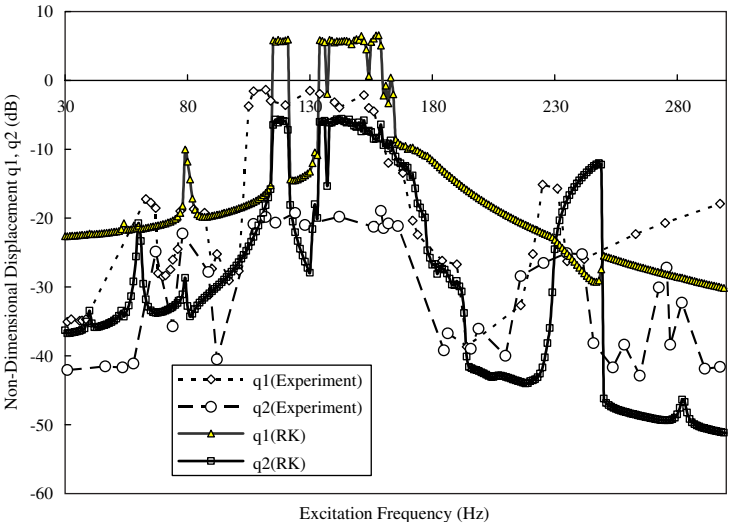

Fig. 13. Modal responses of 4.1 mm ($R_1 = 5.7$) at $32g$.

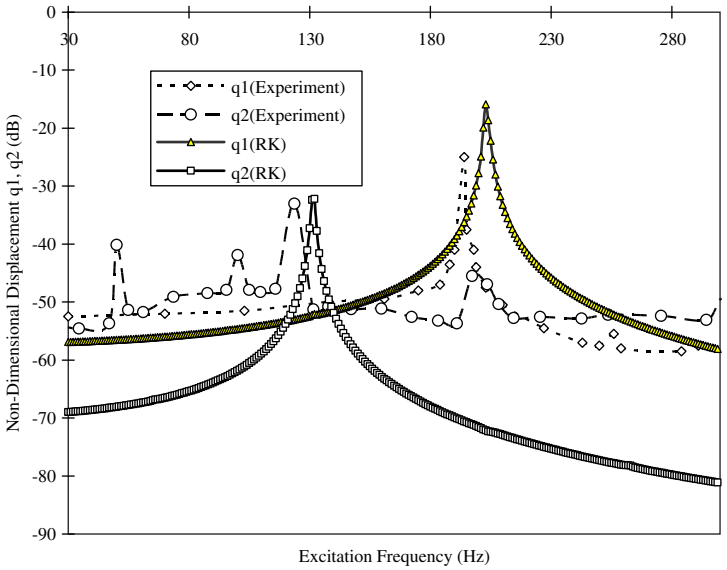

Fig. 14. Modal responses of 5.2 mm ($R_1 = 9$) at $1g$.

outstanding in terms of response magnitude. The measured parametric resonances for the symmetric and antisymmetric modes are quite close to the resonance frequencies under numerical simulation when the excitation level is $1g$ and $4g$. Above these levels, the parametric phenomenon becomes predominant, and the vibration response is chaotic. As the excitation level increases, the width of the parametric resonance increases. For the 5.2-mm deflection ($R_1 = 9$), see Figs. 14–17,

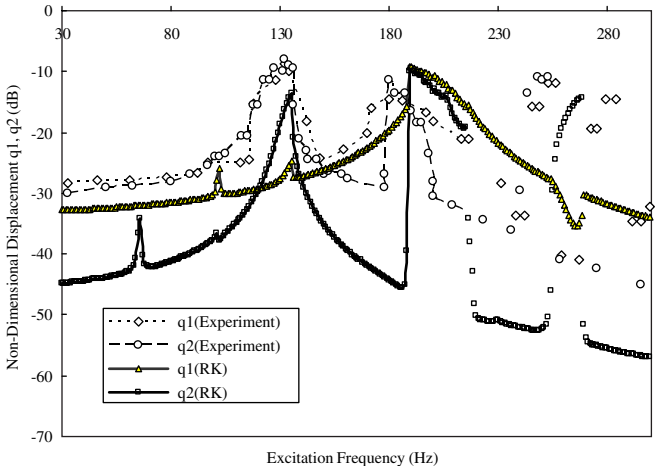

Fig. 15. Modal responses of 5.2 mm ($R_1 = 9$) at 16g.

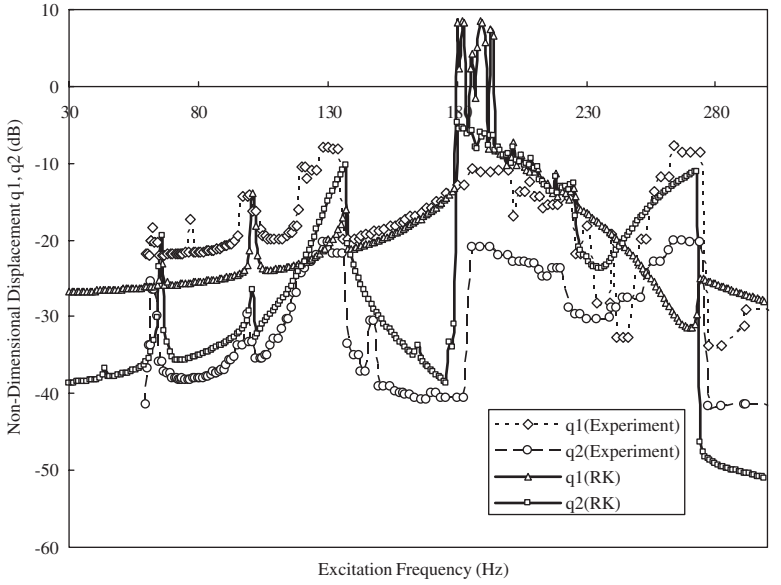

Fig. 16. Modal responses of 5.2 mm ($R_1 = 9$) at 32g.

the ratio of the nonlinear natural frequencies for the first two modes becomes 1.54 near the instability intervals of the autoparametric resonance. However, the response magnitude is comparatively large at 4.1 mm ($R_1 = 5.7$). As mentioned in the previous section, the ideal condition for the presence of autoparametric resonance occurs at a frequency ratio of 2:1. Under this condition, the vibrations of the symmetric system act as a parametric excitation of

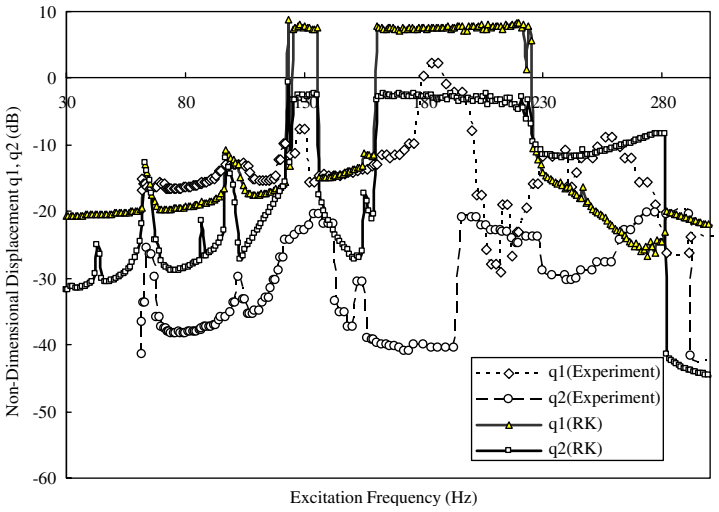

Fig. 17. Modal responses of 5.2 mm ($R_1 = 9$) at $60g$.

the antisymmetric system. The saturation effects are shown in Figs. 12, 13, 15–17. As the excitation level is increased, the symmetric system is given more energy, which results in a strong increase in the deflections of the antisymmetric mode, although the increase of the vibration magnitude of the symmetric mode is much smaller. The data are summarized in Table 2.

The loss of stability of the symmetric mode response of the beam depends on the frequency ratio between the first two modes and the interaction (coupling) between the symmetric and antisymmetric modes. In principle, autoparametric vibration occurs within only a limited region of the system parameters. The autoparametric phenomenon arises if the ratio of the linear resonance frequencies of the symmetric mode and antisymmetric mode are at a ratio of 2:1. Near the region of the 2:1 ratio, the experimental and numerical results show stronger autoparametric instability at $R_1 = 9$ (ratio = 1.56) than at $R_1 = 5.7$ (ratio = 1.33). The response at $R_1 = 5.7$ is of a higher magnitude, because it is closer to the ratio of 2:1. The inevitable slipping effect at the clamps and the variation in nonlinear damping causes the deviation in the response amplitude in the numerical results.

No experiments were conducted for higher deflection cases because the linear resonance frequency of the first mode during the frequency response test was limited to 210 Hz (10 mm beam center deflection) due to energy transfer to the third mode. This phenomenon has been described by Nayfeh [6].

Vertical vibrations of the beam under certain conditions initiate a rotation motion of the antisymmetric mode of the beam through the autoparametric effect. The saturation effect when the symmetric motion of the beam supplies the energy can lead to movement in the antisymmetric mode, which results in a decrease in the excitation force that is required to initiate the dynamic snap-through motion.

Table 2
Summary of the test results

Excitation	Resonance frequencies	Parametric/autoparametric response	Frequency ratio	Occurrence of snap-through
4.1 mm $R = 5.7$				
1g	*1st mode*	*2nd mode*		No
	161 Hz (Exp.)	No	1.33 (Exp.)	Softening
	163 Hz (Num.)		1.35 (Num.)	Spring
	2nd mode			
	121 Hz (Exp.)			
	121 Hz (Num.)			
4g	*1st mode*	*2nd mode*		No
	160 Hz (Exp.)	157 Hz	1.32 (Exp.)	Softening
	158 Hz (Num.)		1.30 (Num.)	Spring
	2nd mode			
	121 Hz (Exp.)			
	122 Hz (Num.)			
16g	*1st mode*	*2nd mode*		No
	134–158 Hz (Exp.)	132–162 Hz (Exp.)	1.39 (Exp.)	Softening
	146–154 Hz (Num.)	148–165 Hz (Num.)	1.25 (Num.)	Spring
	2nd mode			
	114–124 Hz (Exp.)			
	123 Hz (Num.)			
32g	*1st mode*	Instability region at wide		Yes
	107–159 Hz (Exp.)	frequency range	1.48 (Exp.)	Chaotic and
	135–165 Hz (Num.)		1.41 (Num.)	nonperiodic
	2nd mode			
	107–162 Hz (Exp.)			
	117–121 Hz (Num.)			
5.2 mm $R = 9$				
1g	*1st mode*	*2nd mode*		No
	194 Hz (Exp.)	No	1.56 (Exp.)	Softening
	203 Hz (Num.)		1.53 (Num.)	Spring
	2nd mode			
	124 Hz (Exp.)			
	132 Hz (Num.)			
16g	*1st mode*	*2nd mode*		No
	187 Hz (Exp.)	180 Hz (Exp.)	1.52 (Exp.)	Softening
	191 Hz (Num.)	191 Hz (Num.)	1.41 (Num.)	Spring
	2nd mode			
	123–132 Hz (Exp.)			
	135 Hz (Num.)			
32g	*1st mode*	*2nd mode*		No
	186–230 Hz (Exp.)	186–220 Hz (Exp.)	1.54 (Exp.)	Softening
	180–225 Hz (Num.)	180–225 Hz (Num.)	1.64 (Num.)	Spring
	2nd mode			
	121–134 Hz (Exp.)			
	137 Hz (Num.)			

Table 2 (*continued*)

Excitation	Resonance frequencies	Parametric/autoparametric response	Frequency ratio	Occurrence of snap-through
60*g*	*1st mode* 176–196 Hz (Exp.) 162–224 Hz (Num.) *2nd mode* 124–130 Hz (Exp.) 125–135 Hz (Num.)	Instability region at wide frequency range	1.58 (Exp.) 1.79 (Num.)	Yes Chaotic and nonperiodic

5. Conclusions

This is the first known experimental technique to obtain results for the antisymmetric mode of a buckled beam. The effect of the antisymmetric mode of a buckled beam with clamped ends was examined numerically and experimentally. The beam can be tuned into the autoparametric resonance when the natural frequency of the harmonically excited symmetrical mode system is approximately twice the natural frequency of the antisymmetric mode system. Due to the nonlinear modal interaction between the symmetric and antisymmetric modes, the curved beam becomes unstable under parametric excitation.

The theoretical and experimental results conclude that autoparametric responses occur for large static buckled shapes when the resonance frequency of the symmetric mode is about twice that of antisymmetric mode, the autoparametric responses are dominant at a frequency that is half that of the excitation, the autoparametric responses of the antisymmetric modes are as high as the symmetric mode although the excitation force is symmetric, and the autoparametric responses decrease the excitation force that is required to initiate the dynamic snap-through motion. The experimental results for a buckled beam were obtained by base excitation with a 6000 N shaker. The measurement of the antisymmetric modes was separated from that of the symmetric modes through the special configuration of the strain gauge sensor systems. A comparison of the simulation results and measured data shows a reasonable agreement, and demonstrates the effectiveness of the modeling approach.

The autoparametric phenomenon makes the primary region of dynamic instability significantly broader, and thus instabilities occur under smaller forces and a wider range of excitation frequencies.

References

[1] J.J. Thomsen, Chaotic vibrations of non-shallow arches, *Journal of Sound and Vibration* 153 (2) (1992) 239–258.
[2] H. Hatwal, A.K. Mallik, A. Ghosh, Non-linear vibrations of a harmonically excited autoparametric system, *Journal of Sound and Vibration* 81 (2) (1982) 153–164.
[3] A.G. Haddow, A.D.S. Barr, D.T. Mook, Theoretical and experimental study of modal interaction in a two-degree-of-freedom structure, *Journal of Sound and Vibration* 97 (3) (1984) 451–473.

[4] S.I. Chang, A.K. Bajaj, C.M. Krousgrill, Amplitude modulated dynamics in harmonically excited nonlinear oscillations of rectangular plates with internal resonance, in: M. Petyt, H.F. Wolf, C. Mei (Eds.), *Proceedings of the Fourth International Conference on Structural Dynamics: Recent Advances*, Elsevier, London, 1991, pp. 739–748.
[5] A.A. Afaneh, R.A. Ibrahim, Nonlinear response of an initially buckled beam with 1:1 internal resonance to sinusoidal excitation, Nonlinear Vibration ASME1992, DE-Vol.50/AMD-Vol.144.
[6] A.H. Nayfeh, D.T. Mook, *Nonlinear Oscillations*, Wiley Interscience, New York, 1979.
[7] C.L. Liao, B.W. Huang, Parametric instability of a spinning pretwisted beam under periodic axial force, *International Journal of Mechanical Sciences* (1995) 423–439.
[8] T.H. Tan, H.P. Lee, G.S.B. Leng, Parametric instability of spinning pretwisted beam subjected to sinusoidal compressive axial loads, *Computer and Structures* 66 (6) (1998) 745–765.
[9] C.F. Ng, Nonlinear and snap-through responses of curved panels to intense acoustic excitation, *Journal of Aircraft* 26 (3) (1989) 281–288.
[10] C.F. Ng, The nonlinear acoustic response of thermally buckled plates, *Applied Acoustics* 59 (2000) 237–251.
[11] C.F. Ng, Testing techniques for chaotic vibration of buckled aircraft structures, *Proceedings of the Institution of Mechanical Engineers, Part G: Journal of Aerospace Engineering* 210 (1996) 281–290.
[12] C.F. Ng, The analysis of non-linear dynamic behavior (including snap-through) of post-buckled plates by simple analytical solution, NASA Technical Report 181877, 1989.
[13] A.A. Afaneh, R.A. Ibrahim, Nonlinear response of an initially buckled beam with 1:1 internal resonance to sinusoidal excitation, *Nonlinear Dynamics* 4 (1992) 547–572.
[14] W. Kreider, A.H. Nayfeh, Experimental investigation of single-mode responses in a fixed–fixed buckled beam, *Nonlinear Dynamics* 15 (1998) 155–177.
[15] W.Y. Poon, C.F. Ng, Y.Y. Lee, Dynamic stability of a curved beam under sinusoidal loading, *Proceedings of the Institution of Mechanical Engineers, Part G: Journal of Aerospace Engineering* 216 (2002) 209–217.